Dynamic motions of free and bound Ø29 scaffolding protein identified by hydrogen deuterium exchange mass spectrometry

Chi-Yu Fu and Peter E. Prevelige, Jr.

Protein Sci. 2006 15: 731-743; originally published online Mar 7, 2006;
Access the most recent version at doi:10.1110/ps.051921606

Dynamic motions of free and bound Ø29 scaffolding protein identified by hydrogen deuterium exchange mass spectrometry

CHI-YU FU[1] AND PETER E. PREVELIGE JR.[2]

[1]Department of Biochemistry and Molecular Genetics and [2]Department of Microbiology, University of Alabama at Birmingham, Birmingham, Alabama 35294, USA

(RECEIVED October 19, 2005; FINAL REVISION January 7, 2006; ACCEPTED January 13, 2006)

Abstract

In the double-stranded DNA containing bacteriophages, hundreds of copies of capsid protein subunits polymerize to form icosahedral shells, called procapsids, into which the viral genome is subsequently packaged to form infectious virions. High assembly fidelity requires the assistance of scaffolding protein molecules, which interact with the capsid proteins to insure proper geometrical incorporation of subunits into the growing icosahedral lattices. The interactions between the scaffolding and capsid proteins are transient and are subsequently disrupted during DNA packaging. Removal of scaffolding protein is achieved either by proteolysis or alternatively by some form of conformational switch that allows it to dissociate from the capsid. To identify the switch controlling scaffolding protein association and release, hydrogen deuterium exchange was applied to *Bacillus subtilis* phage Ø29 scaffolding protein gp7 in both free and procapsid-bound forms. The H/D exchange experiments revealed highly dynamic and cooperative opening motions of scaffolding molecules in the N-terminal helix-loop-helix (H-L-H) region. The motions can be promoted by destabilizing the hydrophobic contact between two helices. At low temperature where high energy motions were damped, or in a mutant in which the helices were tethered through the introduction of a disulfide bond, this region displayed restricted cooperative opening motions as demonstrated by a switch in the exchange kinetics from correlated EX1 exchange to uncorrelated EX2 exchange. The cooperative opening rate was increased in the procapsid-bound form, suggesting this region might interact with the capsid protein. Its dynamic nature might play a role in the assembly and release mechanism.

Keywords: bacteriophage Ø29; scaffolding proteins; virus assembly; helix-loop-helix structure; hydrogen deuterium exchange; EX1 exchange; mass spectrometry

Supplemental material: see www.proteinscience.org

Viruses assemble protein shells called capsids, which surround the viral genome and protect it from environmental insult. To minimize the fraction of the viral genome dedicated to specifying the capsid, the protein shells are usually built from multiple copies of a small number of protein subunits. Conserved or quasi-equivalent bonding interactions between protein subunits lead to regular and symmetrical final structures such as helices and icosahedra (Caspar and Klug 1962). For some icosahedral viruses, such as the T = 3 plant viruses, the capsid proteins copolymerize with the viral genome, leading to concerted assembly and packaging (Casjens and King 1975). An alternative strategy utilized by the bacteriophage and herpes virus is one in which the capsid proteins first assemble into metastable procapsid structures. The genome is subsequently packaged in an

Reprint requests to: Peter E. Prevelige Jr., Department of Microbiology, University of Alabama at Birmingham, BBRB 416 845 19th St. South, Birmingham, AL 35294-2170, USA; e-mail: prevelig@uab.edu; fax: (205) 975-5479.

Abbreviations: H/D exchange, hydrogen deuterium exchange; H-L-H structure, helix-loop-helix structure.

Article published online ahead of print. Article and publication date are at http://www.proteinscience.org/cgi/doi/10.1110/ps.051921606.

ATP-dependent process through a unique vertex of the icosahedron at which the capsid proteins are replaced by a dodecamer of a specialized portal protein (Bazinet and King 1985; Casjens and Hendrix 1988; Homa and Brown 1997).

The assembly of well-dimensioned procapsids requires that the capsid protein copolymerize with a scaffolding protein. Based on a variety of biophysical and biochemical data, two functions for scaffolding proteins have been suggested. First, they lower the energy barrier for nucleation of polymerization, resulting in a decreased critical concentration. Second, they ensure proper form determination by positioning the capsid protein subunits relative to one another in the icosahedral shells (King et al. 1973; Prevelige et al. 1993). In the absence of scaffolding protein, aberrant spirals dominate the assembly reactions. These spirals presumably result from inappropriate relative positioning of the hexameric and penatmeric capsomeres required to build a capsid with >60 subunits (Berger et al. 1994).

Most scaffolding proteins are elongated molecules with high α-helical content (Dokland 1999). During assembly scaffolding proteins interact with capsid proteins and drive the protein polymerization in a defined pathway. During DNA packaging the interactions between scaffolding and capsid proteins need to be disrupted to allow the scaffolding proteins to be released, thereby leaving room for the viral genome (Earnshaw and Casjens 1980). One mechanism of release is proteolytic destruction of the binding site. For example, in Herpes Simplex Virus type 1, the C-terminal residues of scaffolding protein interact with capsid protein. The scaffolding protein itself contains a serine protease, which cleaves the C-terminal 25 amino acids of scaffolding protein, resulting in its release from the capsid (DiIanni et al. 1994; Homa and Brown 1997). However, in some phages, the scaffolding proteins are released intact during DNA packaging, suggesting destruction of the binding site arises through conformational changes. While DNA packaging is accompanied by changes in the coat protein lattice, which could account for release in some phage, this is apparently not universal. It is equally likely that the scaffolding protein itself can adopt different conformations to switch between bound and free forms.

Because of their extended and flexible helical character, scaffolding proteins have proven difficult to crystallize. The capsid protein binding domain of the scaffolding protein from the *Salmonella typhimurium* bacteriophage P22 is situated at the C terminus of the protein. The NMR structure of the binding site consists of a helix-loop-helix (H-L-H) motif (Parker et al. 1998; Sun et al. 2000). Recently, the crystal structure of the scaffolding protein from the *Bacillus subtilis* phage Ø29 was solved (Morais et al. 2003). The Ø29 scaffolding protein consists of three α-helices and a disordered C terminus. As do many scaffolding proteins, the protein forms dimers in solution and the crystal structure reveals that dimerization is mediated by a leucine zipper motif at the C-terminal α-helix 3. The N-terminal region adopts a helix-loop-helix structure that is homologous to the C-terminal capsid binding domain of P22 scaffolding protein.

One possible mechanism for Ø29 scaffolding protein function is that the unstructured C terminus becomes structured upon interacting with capsid proteins; the capsid binding domains are situated in the C-terminal region of the protein in many phage (Fane and Prevelige 2003). Alternatively, as proposed by Morais et al. (2003), it is possible that the N-terminal H-L-H represents the capsid binding site.

To identify conformational differences between free and procapsid-bound scaffolding protein, hydrogen deuterium exchange was employed. This technique monitors the exchange rate of amide protons with solvent. The amide proton exchange rate is dependent on both chemical and structural factors (Kaltashov and Eyles 2002; Hoofnagle et al. 2003).

At physiological pH an exposed amide proton can exchange with protons or deuterons from solvent through a base catalyzed reaction. The chemical exchange rate (k_{ch}) is determined by the concentration of hydroxyl groups and an intrinsic rate constant (k_{int}) that depends on both temperature and amino acid sequence (Molday et al. 1972):

$$k_{ch} = k_{int}[OH^-]$$

Because proton abstraction cannot occur if the proton is hydrogen bonded, the observed exchange rate (k_{ex}) in a structured protein also depends on the opening and closing rates of the H-bond (k_{op}, k_{cl}). These rates are affected by protein structure and stability, thus providing structural information.

$$k_{ex} = (k_{op} \times k_{ch}) / (k_{cl} + k_{ch})$$

Exchange conditions where $k_{cl} << k_{ch}$ are known as the EX1 regime. Under these conditions, every opening event results in full exchange of the opened region and, therefore, the observed exchange rate represents the opening rate (Hilton and Woodward 1979; Ferraro et al. 2004):

$$k_{ex} = k_{op}$$

Conditions where $k_{cl} >> k_{ch}$ are known as the EX2 regime. Under these conditions repeated cycles of opening

and closing are required for full exchange and therefore:

$$k_{ex} = (k_{op} / k_{cl}) / k_{ch} = K_{op} \times k_{ch}$$

$$\Delta G_{ex} = -RT \ln K_{op}$$

One advantage of employing mass spectrometry to monitor exchange experiments is its ability to discriminate between these two regimes (Ferraro et al. 2004). Regions undergoing EX1 exchange will show a bimodal distribution of mass in which the mass difference between the two peaks corresponds to the number of amide protons in the cooperative opening unit, and the time dependence of the shift to higher mass corresponds to the opening rate. In the case of the EX2 regime, a unimodal peak that continuously shifts from low mass to high mass over time will be observed. A second advantage of using mass spectrometry to detect H/D exchange measurements is its ability to follow exchange kinetics in large supramolecular structures (Hernandez and Robinson 2001; Lanman and Prevelige 2004). Here, we compare the H/D exchange kinetics of free and bound scaffolding protein to identify dynamic regions within the scaffolding protein and demonstrate that the dynamics of these regions change upon interaction with the capsid protein.

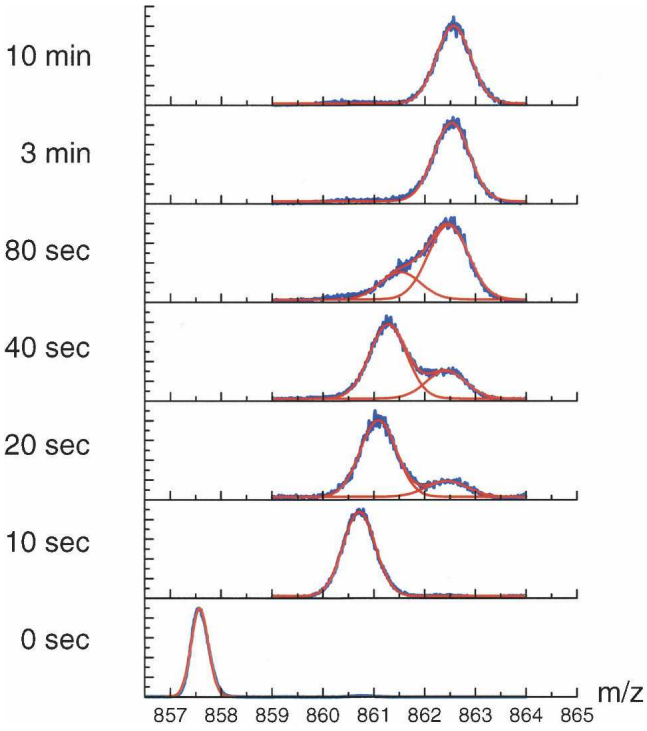

Figure 1. The hydrogen deuterium exchange profile of scaffolding protein at room temperature. Recombinant scaffolding protein was exchanged in D_2O buffer at room temperature. The reactions were quenched at various time points as indicated. The mass spectra show the mass to charge ratio of the 13+ charge state of scaffolding proteins from 0 to 10 min exchange times (blue line). The raw spectra were fit with either one (0, 10 sec, 3 min, 10 min of exchange) or two (20 sec, 40 sec, 80 sec of exchange) Gaussian distributions as necessary to describe the deuterated states (red line).

Results

Scaffolding protein exchanges bimodally at room temperature

In order to compare the H/D exchange profiles of free and procapsid-bound forms of scaffolding protein, the H/D exchange of free scaffolding was first examined using recombinant proteins purified from *Escherichia coli*. Exchange was carried out at room temperature and initiated by diluting recombinant scaffolding 10-fold into D_2O buffer to a final concentration of 20 μM. At this protein concentration the scaffolding protein is essentially completely dimeric as determined by sedimentation equilibrium analysis. The exchange reaction was quenched at various time points by adding a fourfold volume of 2% formic acid to a final pH of 2.5. The samples were immediately flash-frozen in liquid nitrogen. The global deuterium uptake was subsequently analyzed by ESI-TOF mass spectrometry.

The mass spectrum of the 13+ charge state of scaffolding protein before exchange consists of a single peak centered at 857.58 *m*/*z* (Fig. 1, bottom panel). The 13+ charge state represents the dominant charge state in an envelope that spanned 10+ to 16+ charges. The average mass of 11,136 Da, derived by maximum entropy fitting of the multiple-charged species, agrees well with the average mass expected from the known amino acid composition of 11,135 Da. The resolving power of ESI-TOF mass spectrometry is insufficient to resolve the isotopic distribution within individual charge states (0.077 *m*/*z* spacing between isotopes in the 13+ charge state). The isotopic distribution follows a binomial distribution but can be well approximated by a Gaussian distribution (Chung et al. 1997). After 10 sec of exchange in D_2O buffer (Fig. 1), the 13+ charge peak shifts from 857.58 to 860.71 *m*/*z*, a shift corresponding to the uptake of 40 deuterons. The peak shape is still well described by a single Gaussian distribution but the peak width is broadened compared with the spectrum before exchange as a result of the binomially distributed incorporation of deuterium within the population of scaffolding molecules. The residues that exchange on this time scale are generally thought to correspond to rapidly exchanging surface residues (Mandell et al. 1998).

Exchange is essentially complete after 10 min as witnessed by the fact that there is no further exchange after

30 h. In both cases, the distribution consists of a single peak centered at 862.56 m/z (11,200 Da). The observed mass shift corresponds to the uptake of a total of 64 deuterons. Scaffolding protein has 94 exchangeable amide protons. In 90% D_2O the fully exchanged protein would be expected to have 85 deuterons. We therefore estimate that back exchange was ~25%. The fact that the protein was essentially completely exchanged after only 10 min is consistent with the fact that the crystallographically determined structure of scaffolding protein lacks a substantial well-folded core (Morais et al. 2003).

At intermediate exchange times (from 20 to 80 sec) (Fig. 1), the mass spectra display a clear shoulder. To semi-quantitatively analyze the data, the spectra were fit with Gaussian distributions. The unexchanged, fully exchanged, and 10-sec data points were well fit by a single Gaussian, while the spectra taken between 20 and 80 sec required two Gaussian distributions for a satisfactory fit (Fig. 1). Between 10 and 20 sec of exchange, the major peak shifts from 860.71 to 861.08 m/z, corresponding to the incorporation of ~5 deuterons. After this initial shift, the center of the lower mass distribution showed a very slight increase over time (861.08, 861.27, and 861.52 m/z at 20, 40, and 80 sec, respectively). The center of the higher mass peak was relatively constant (862.44, 862.41, and 862.46 m/z at 20, 40, and 80 sec, respectively) and was close to the fully exchanged state value of 862.56. While the centers of the Gaussian peaks do not shift significantly over time, their relative areas do. From 20 to 80 sec, the area under the lower mass distribution decreases while the area under the higher mass species increases from 19% to 28% to 73%. The relative shift between two deuterated states without populating intermediates is classified as EX1 exchange. In this exchange regime, the closing rate of the structure is far smaller than the chemical exchange rate. Thus, the residues exchange cooperatively when the structural unit opens and becomes fully exchanged before closing again. In a pure EX1 exchange reaction, the positions of the peak centers are unchanged while the area underneath varies as the function of exchange time. The rate of change in the area under the higher mass peak represents the opening rate of the structural unit. To quantify the opening kinetics, the relative area under the higher mass peak was calculated and plotted versus the exchange time (see Fig. 3B, below). The slight shift observed in our data for the lower mass peak (3.3 Da between 20 and 40 sec; 4.3 Da from 40 sec to 1.2 min) may arise from small amounts of deuterium uptake in other regions of the protein. The mass differences between the lower and higher mass peaks range from 16 to 23 Da over time after correction for back exchange, suggesting that the size of the protected interface that exposes and exchanges in cooperative opening motions is ~16–23 Da.

The N-terminal helix-loop-helix motif exchanges as a structural unit

To get region specific exchange information and to identify the bimodal region, a pepsin digestion step was performed after the quench. Because exchange broadens the isotopic envelopes resulting in mass overlap, the resultant peptides were partially separated by reverse phase chromatography at 4°C using a rapid acetonitrile gradient in the presence of formic acid. Ninety-five percent peptide coverage was obtained. Three fragments corresponding to residues 1–19, 20–31, and 32–38 displayed bimodal exchange profiles. Figure 2A shows the exchange profile of a triply-charged peptide corresponding to residues 1–19. The bottom trace shows the peptide prior to exchange in which the 1-Da mass increment peaks arising from the natural isotope incorporation are resolved with a spacing of 0.33 Da. The top panel of Figure 2A shows the fully exchanged spectrum at 10 min. Between 20 sec and 1 min, the spectra show a broadening of the isotopic distribution compared with that of the 10-min time point.

To semi-quantitatively analyze the data, the centroid of each isotopic peak was calculated and plotted (Fig. 2D), and the resultant distribution was fitted with either one or two Gaussian distributions as necessary. The lower mass Gaussian envelopes at the 20-sec, 40-sec, and 1-min time points are centered at 749.62, 749.96, and 750.18 m/z, respectively, with shifts of 1.4 and 0.9 Da between the time points after correction for 27% back exchange. The higher mass envelopes at the 40-sec, 1-min, 3-min, and 10-min time points are centered at 751.42, 751.50, 751.62, and 751.68 m/z, respectively, with shifts of 0.3, 0.5, and 0.2 Da. The data suggest that there is a rapid uptake of an average of 5 deuterons within 20 sec. This likely corresponds to surface residues. This is followed by the cooperative opening of a protected structural unit resulting in the observed bimodality. The size of the structural unit (5.4–6.0 amide protons) corresponds to 38% of total exchangeable amides in residues 1–19, or about one-third of the helix. A slight shift (0.2–1.4 Da) of both the lower and higher mass envelopes is seen over time, which likely represents uptake through additional local bond breaking in the structure (Canet et al. 2002).

Figure 2B shows the spectra of the doubly-charged peptide spanning residues 20–31 (1373.10 Da). The 20-sec, 40-sec, and 1-min time points also appear to have a broadened distribution compared with that of the 10-min time point. When fit with one or two Gaussian peaks as required (Fig. 2E), it shows a pattern of exchange similar to that of residues 1–19 in which two Gaussians are required to fit the distribution at intermediate times. The centers of those Gaussians also show slight shifts of 0.3–1.0 Da toward increased mass over time. There is a difference of ~4.2 deuterons between the two

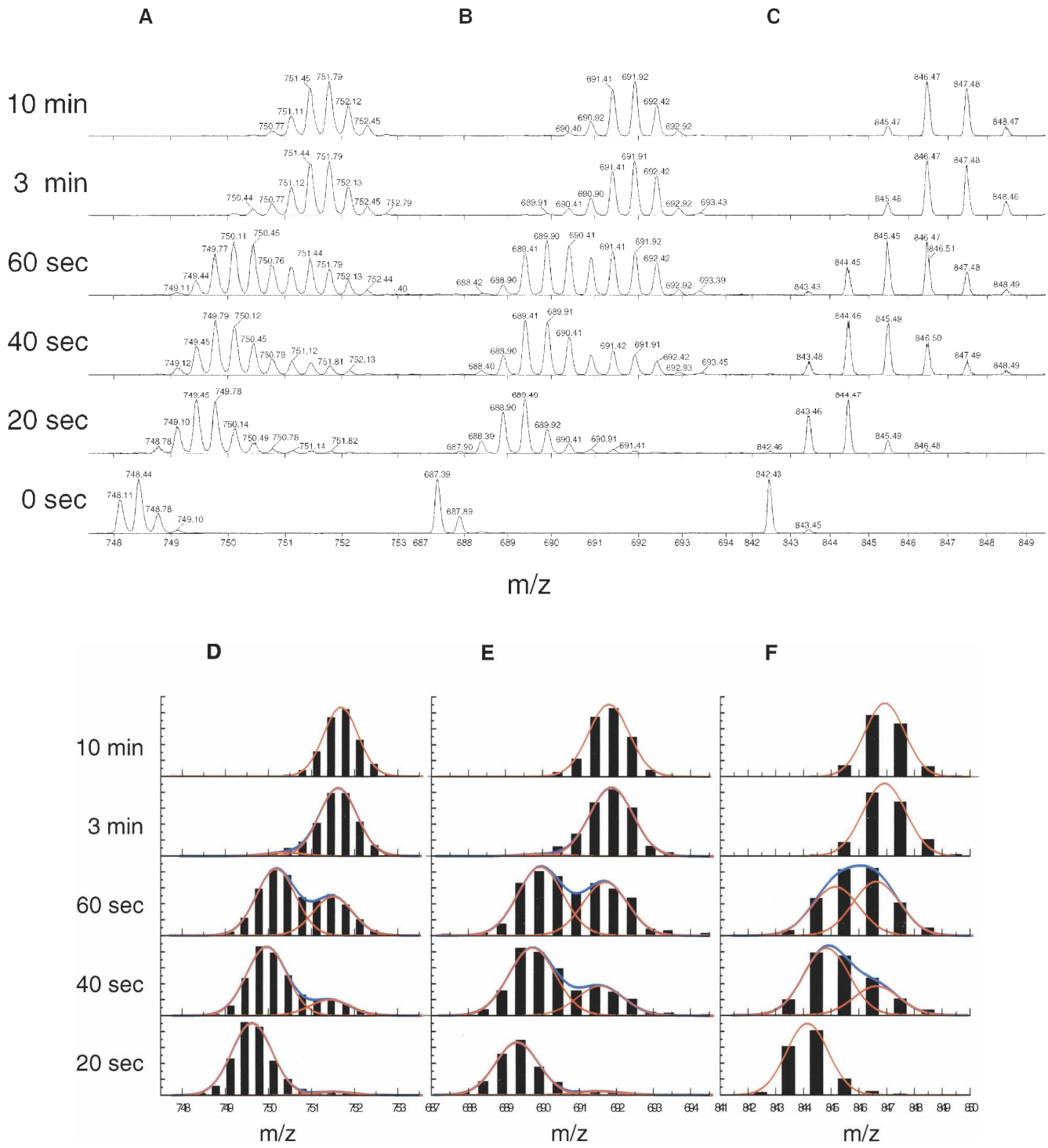

Figure 2. The isotopic distributions of peptides derived from the N-terminal H-L-H region. The isotopic distributions of residues 1–19 (*A*), residues 20–31 (*B*), and residues 32–38 (*C*) at exchange periods ranging from 0 to 10 min. The area under each isotopic peak in *A*, *B*, and *C* is represented by the black bar as plotted in *D*, *E*, and *F*, respectively. The resultant distributions were approximated with either one or two Gaussian distributions as required (red line). The sum of two Gaussian distributions is plotted in blue as an indicator of the quality of the fit.

states, which indicates that ~38% of the residues in this peptide are in the protected interface. A similar pattern is observed for the singly-charged peptide corresponding to residues 32–38 (841.45 Da) (Fig. 2C,F). On average, two out of six residues are in the protected interface as derived from mass differences between two Gaussian envelopes.

The relative fraction of area under the higher mass Gaussian peak for the whole protein and for each of the peptides contained within residues 1–38 was plotted versus exchange time (Fig. 3B). They all showed similar opening kinetics suggesting that the H-L-H motif is a dynamic cooperative structural unit. No other bimodally exchanging peptides were identified.

The opening motions can be frozen by lowering the temperature

If the observed bimodality originates from a high-energy cooperative opening motion of the H-L-H motif, lowering the temperature will preferentially slow that motion. In the limit, the cooperative opening will be completely frozen and exchange will occur through small, uncoupled low-energy local motions resulting in an EX2-type exchange pattern. Therefore, exchange was performed at lower temperatures.

Lowering the temperature also decreases the chemical exchange rate. Because observing EX1-type exchange requires that the chemical exchange rate be much faster than the closing rate, it is necessary to hold the chemical exchange rate constant as the temperature is decreased. This was accomplished by increasing the pH of the exchange reaction, which has the effect of increasing general base catalyzed exchange (Molday et al. 1972). Under these conditions, differences seen at different temperatures will only reflect the temperature effect on structural dynamics. pH adjusted exchange experiments were performed at 20°C, 10°C, and 4°C.

Figure 4A shows the centered spectra of residues 20–31 in the H-L-H region. At 20°C, scaffolding protein still exchanges bimodally but has a delayed bimodal window. Whereas at room temperature (~24°C) bimodality first becomes evident at 20 sec and is resolved after ~3 min, at 20°C the window spans 3–7 min. The fully exchanged envelope is centered at 690.46 *m*/*z*, which is somewhat lower than the value obtained in Figure 2D due to increased back exchange arising from sample handling differences that were necessitated by the analysis of procapsid-bound scaffolding (see below). The isotopic distribution at the 3- to 7-min exchange times were described by Gaussian fits (Fig. 4A). At 20°C, the H-L-H still exchanges cooperatively, indicating that the closing rate remains slow relative to the chemical exchange rate. The mass difference of an average 4.4 Da between lower and higher mass states (after correction for back exchange) is similar to that seen at room temperature, indicating that the size of the cooperative unit is unaffected by temperature, but the opening rate has been slowed, resulting in a decreased rate of deuterium incorporation.

At both 10°C and 4°C, the exchange envelopes were well described by a single Gaussian that migrates toward 690.38 *m*/*z* over time (Fig. 4B). About the same number of deuterons is taken up by surface residues at 20 sec for all three temperatures, and all three reactions reach the same end point after 30 h. EX2-like exchange occurs at 10°C and 4°C. Under these conditions, the opening rate for the cooperative motions has become so slow that exchange from the low energy local EX2-type motions dominates the exchange profile.

The dimer interface is more protected at 4°C

The regions outside the H-L-H motif all exchange unimodally at all three temperatures. For each peptide, the centroid of the isotopic distribution was calculated at

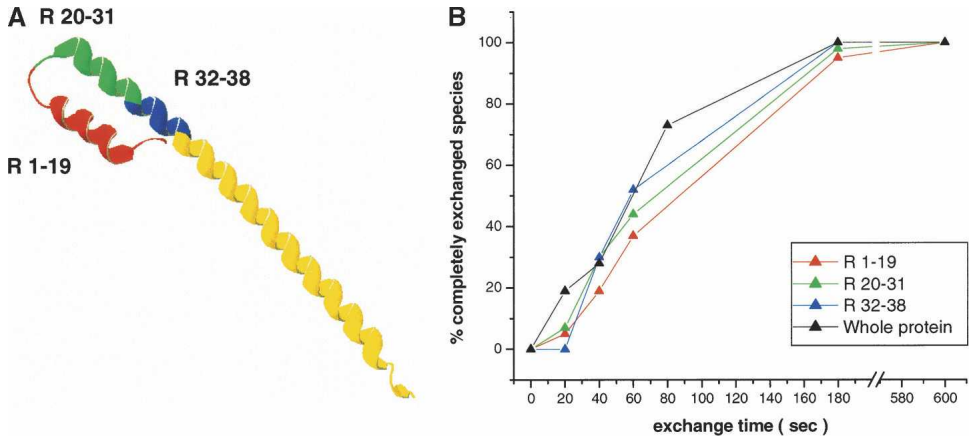

Figure 3. The opening kinetics of the N-terminal helix-loop-helix motif. (*A*) The peptides that displayed a bimodal exchange profile are color-coded onto the crystallographically determined structure (1NO4): (Red) Residues 1–19, (green) residues 20–31, (blue) residues 32–38. (*B*) To compare the opening kinetics of different regions, the fraction of total area represented by the higher mass peak in the whole protein and the individual peptides at each time point was calculated and plotted as the function of exchange time.

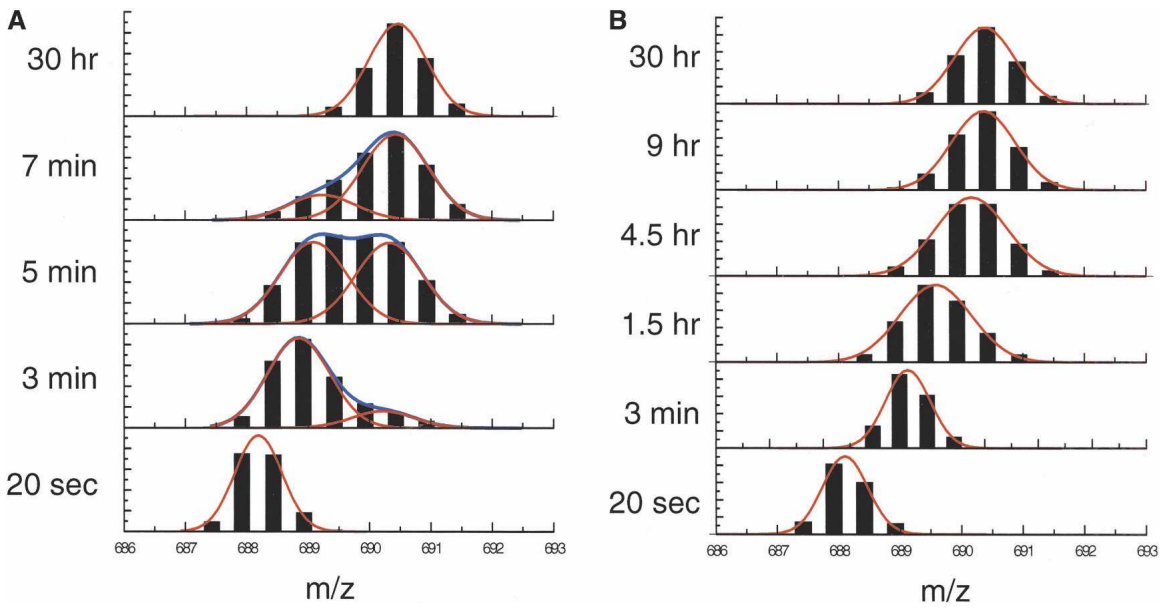

Figure 4. The effect of temperature on H-L-H motions. (*A*) The isotopic peaks of residues 20–31 exchanging at 20°C are represented by black bars. Two Gaussian distributions (red line) were required to approximate the envelopes of the 3- to 7-min exchange times at 20°C with the sum of the two envelopes as shown in blue. (*B*) The isotopic peaks of residues 20–31 exchanging at 10°C. One Gaussian distribution (red line) was sufficient to describe the isotopic envelope for all exchange time points.

each time point and the progress curve fit as a sum of three exponentials. Figure 5A shows the deuterium uptake over time for residues 39–59, which is part of helix 3 and forms a dimeric contact in the crystal structure. At 20°C, 13.6 and 6.4 residues are classified in the fast ($k > 1\ min^{-1}$) and medium ($1\ min^{-1} > k > 0.01\ min^{-1}$) exchanging categories, respectively. At 10°C, 12.4 and 7.6 are in the fast and medium exchanging categories. However, at 4°C, while 7.1 residues are still in the fast exchanging category, 12.9 residues enter the slowly exchanging category ($k < 0.01\ min^{-1}$). At 20°C, it is likely that two-thirds of the residues pointing outward constitute the fast exchanging class while the one-third pointing toward the dimer interface constitute the medium exchange class. At 10°C, a few additional residues enter the medium exchanging class, perhaps corresponding to

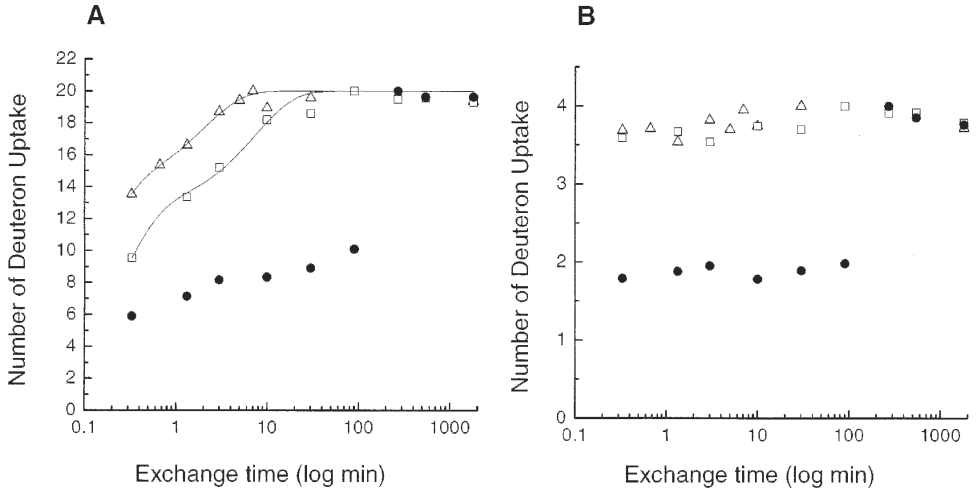

Figure 5. The effect of temperature on the exchange of helix 3. Exchanges on scaffolding proteins were carried out at 4°C, 10°C, and 20°C. The centroid of isotopic distributions of residues 39–59 (*A*) and residues 62–66 (*B*) was calculated and the number of deuteron uptake after correcting for back exchange was plotted vs. exchange time in log scale. The data of 4°C, 10°C, and 20°C exchange are shown by circles, squares, and triangles, respectively. Exponentials with three components were used to classify the residues in fragment 39–59 to fast, medium, and slow exchanging categories at 10°C and 20°C exchange (line).

those residues adjacent to the interface. At 4°C, approximately two-thirds of the residues have entered the slowly exchanging class. There are two limiting explanations for this phenomenon. One possibility is that the interactions between the subunits of the dimer are strengthened by low temperature leading to increased protection of residues situated at or close to the interface. The other possibility is that the low temperature results in a generalized decrease in the uncorrelated breathing motions within the helical regions and, thereby, the overall exchange rate. While we cannot discriminate between these possibilities without residue specific exchange information, we favor the latter because the scaffolding protein dimers have nanomolar affinity. Therefore, it seems less likely that the interfacial contacts will be substantially strengthened at low temperature and more likely that strengthening of hydrogen bonds within the helix at 4°C causes the increased protection (Cordier and Grzesiek 2002).

In contrast to the N-terminal two-thirds of helix 3, which show protection, none of a series of peptides that span the last three helical turns and the C-terminal 15 residues displayed protection (see, for example, Fig. 5B). While the C-terminal 15 residues are disordered in the crystal structure and might not be expected to show protection, the last three turns of helix 3 appear to contribute to the dimer interface. The rapid exchange of these residues suggests that they might not contribute significantly to dimer stability. The effect of these residues on dimer formation was determined by sedimentation equilibrium analysis. A mutant truncated after residue 61 was constructed, expressed, purified, and analyzed by global fitting of sedimentation equilibrium data from three concentrations and three rotor speeds (Supplemental Fig. 2). Because the intact protein forms a tight dimer, in an effort to populate the monomeric form these experiments were done at the lower limit of protein concentration detectable by absorbance optics at 230 nm. The equilibrium data was well fit by a single species whose molecular weight corresponded to the dimer, indicating that the truncated protein still forms a tight dimer. A second mutant was constructed in which the entire helix 3 was deleted. Equilibrium sedimentation analysis demonstrated that this protein also remained capable of dimerizing, presumably through H-L-H contacts, although it had a dissociation constant of 40 μM (Supplemental Fig. 3).

The intramolecular H-L-H interface opens and exchanges cooperatively

The cooperative opening motion detected in the H-L-H region could arise from either opening the H-L-H itself or breaking the intermolecular contacts between H-L-H motifs seen in the dimer structure (Morais et al. 2003). To distinguish the origin of the bimodality, cysteine substitutions were engineered into residues 3 and 35, which were predicted by computer modeling to form a disulfide bond and tether the H-L-H motif. If the bimodality arises from opening of the H-L-H motif, the bimodality will be abolished when the cooperative opening motion in the oxidized form of the double cysteine mutant is restricted, and exchange will then follow EX2 regime.

The double cysteine mutant protein was expressed and purified. As determined by reactivity toward Ellman's reagent, 95% of the mutant scaffolding protein was in the oxidized state after purification. The reduced form was obtained by adding 5 mM DTT. In the absence of DTT a disulfide linked fragment composed of residues 2–10 cross-linked to 31–37 was observed in a tryptic digest. This peptide disappeared upon DTT treatment indicating reduction had occurred.

The reduced form was exchanged in D_2O buffer plus 5 mM DTT. It was completely exchanged within 10 sec at 20°C (data not shown) and therefore shows less protection than the wild-type protein, perhaps due to a slight structural perturbation. To slow the thermal motions, the exchange temperature was lowered to 10°C. Figure 6A shows the spectra of residues 20–31. At 10°C the reduced form exchanges bimodally with Gaussian-approximated lower and higher mass peaks at 688.32 and 690.52 m/z, indicating cooperative opening motions.

In contrast, when the oxidized form was exchanged under identical conditions, the exchange profile of residues 20–31 was well described by a single Gaussian peak that migrates through intermediate states and completes exchange within 10 min (Fig. 6B). Thus, when the H-L-H motif is tethered together, the deuterium uptake is through the local breaking of individual hydrogen bonds instead of the coordinated opening of the motif. In the reduced form in which the motif can still open freely, the fully deuterated species is populated after 10 sec of exchange, whereas no fully exchanged species is evident in the oxidized form. This suggests the interface that is protected from exchange in the oxidized form is opened and accessible in the reduced structure and that the origin of bimodality is from cooperative opening and exchange within the H-L-H motif.

Reducing the hydrophobic contact in the H-L-H motif increases the opening kinetics

To alter the opening kinetics, mutations were introduced to destabilize the closed state of H-L-H by reducing the hydrophobic interactions between helix 1 and helix 3. Proline 2 was mutated to glycine, which was expected to weaken the interaction with phenylalanine 39. The mutant

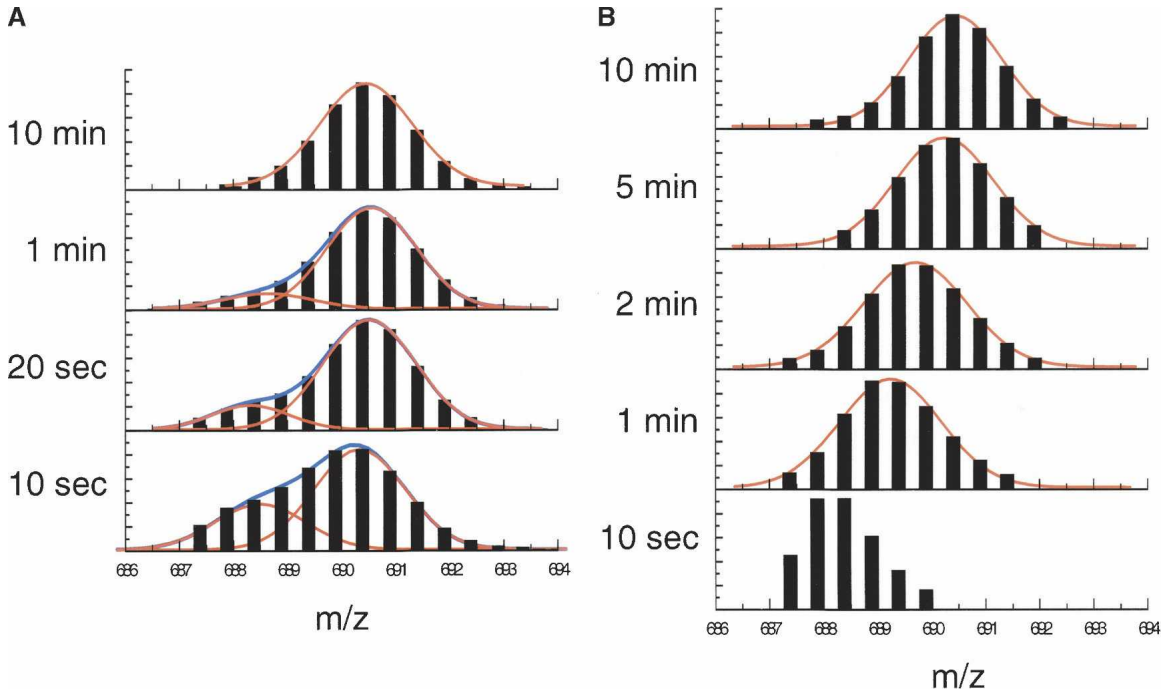

Figure 6. The effect of restricted H-L-H opening motions on the bimodal exchange pattern. Exchanges on double cysteine mutants in both reduced and oxidized forms were performed at 10°C. (*A*) The isotopic peaks of residues 20–31 of reduced form are shown with black bars. Two Gaussian distributions were required to describe the 10 sec, 20 sec, and 1 min of exchange (red line). (*B*) In the oxidized form, a single Gaussian envelope well approximated the distribution from 10 sec of exchange to the completion.

scaffolding in free form was purified and exchanged in D_2O buffer at 10°C. Figure 7 shows the exchange profiles of residues 20–31 of P2G scaffolding from 20 sec to 10 min. In this construct, the bimodal window occurs from 20 sec to 5 min with the lower and higher mass envelopes centered at 688.57 and 690.61 *m*/*z*, respectively. The exchange profile of wild-type protein at 20 sec (Fig. 7, bottom trace) has the same distribution as the low mass species of the P2G mutant, suggesting that the surface residues in both P2G mutant and wild type exchange similarly and give rise to the lower mass deuterated species. However, at 20 sec the P2G mutant displays a rapidly exchanging component not seen in the wild type even after 10 min. In P2G, the fast exchanging species becomes more populated through 5 min and all converge at 690.54 *m*/*z* at 10 min. Based on the exchange kinetics, the H-L-H region in the P2G mutant has a stability that is intermediate between that of the wild-type protein and the reduced form of disulfide tethered variant (L3C/N35C). Other two hydrophobic pairs between helix 1 and helix 3 were mutated to reduce the hydrophobic interaction (Ile11/Leu32 to Ala11/Ala32 and Leu15/Ala28 to Ala15/Gly28). These mutant proteins also show faster exchange kinetics than wild-type protein (data not shown). The data indicate that hydrophobic interactions stabilize the H-L-H contact and the reduced hydrophobic interactions between helix 1 and helix 3 result in faster opening kinetics of the motif.

Procapsid-bound scaffolding protein displays faster opening kinetics

To identify the conformational changes of scaffolding protein upon binding to the capsid, hydrogen deuterium exchange of free scaffolding proteins and scaffolding protein within procapsid particles were compared. Procapsid particles at 1 μM were diluted 10-fold into D_2O buffer and quenched at various time points. Under quench conditions, no scaffolding protein was detected in the pellet after high-speed centrifugation, indicating that the quench conditions release all the scaffolding protein from the capsids. Therefore, the signal seen in the mass spectrometry represents the entire scaffolding protein population. Exchange was carried out at room temperature. Both free and procapsid-bound scaffolding proteins have similar exchange patterns, with 16.3–23.6 Da differences between bimodal peaks through 20–80 sec. To detect changes in a region specific manner, pepsin digestion was performed after the quench. Ninety-five percent coverage was obtained for both samples.

In most regions, both free and bound scaffolding proteins have similar exchange kinetics. The only

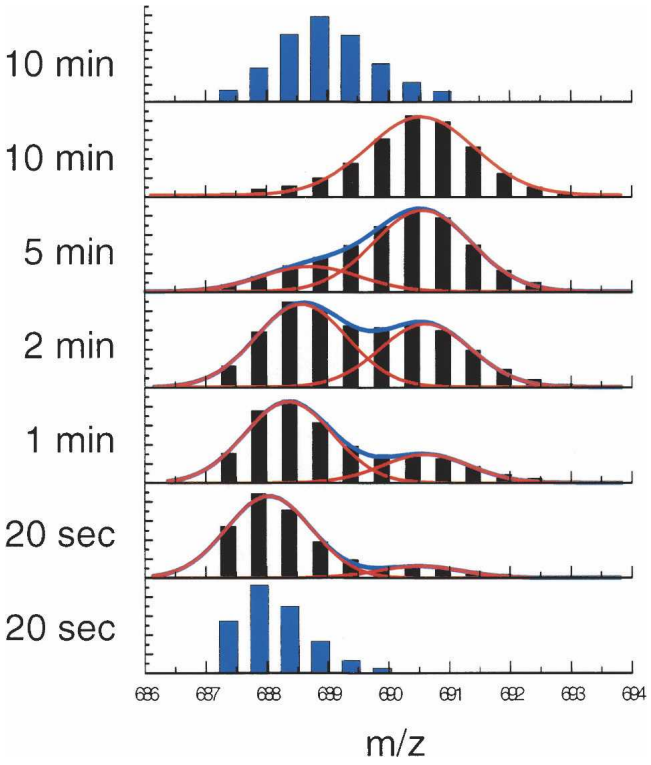

Figure 7. The effect of hydrophobic interactions between helix 1 and helix 3 on opening kinetics. Exchanges on wild type and P2G mutant were done at 10°C. The isotopic distributions of residues 20–31 were plotted in black for P2G mutant exchanging from 20 sec to 10 min. Two deuterated states were approximated by Gaussian, as shown by red lines. The *bottom* and *top* panels show in blue the 20-sec and 10-min exchange spectra of the same peptide from wild type.

difference seen is in residues 20–31 and the difference depends on the scaffolding content of the procapsid particles. Figure 8, A and B, shows the centered spectra of residues 20–31 of the free and procapsid-bound scaffolding protein (with a 3:100 scaffolding protein:capsid protein ratio). A Gaussian approximation was used to describe the lower and higher mass envelopes in the bimodal peak. The fraction of the total area underneath the higher mass envelope was plotted as a function of exchange time (Fig. 8C). The rate of the shift of area, from the lower to higher mass peak, reflects the rate of opening of the structural unit. The procapsid-bound scaffolding shows faster opening kinetics relative to the free form. No differences were seen in other H-L-H-derived peptides. Scaffolding protein in procapsids with higher scaffolding content (11 scaffolding to 100 capsid protein) has similar observed kinetics in residue 20–31 as free forms (Fig. 8C). Five different procapsid preparations with different scaffolding content ranging from 3–11 scaffolding to 100 capsid protein follow the same trend. The data suggest there are two populations of scaffolding in procapsids: one population that displays increased cooperative exchange and one population that does not. At low scaffolding-to-coat ratios the scaffolding binding results in enhanced exchange, but once this population is saturated with additional molecules, it does not show enhanced exchange.

Discussion

The interaction of scaffolding proteins with coat protein subunits is required for proper form determination during viral capsid assembly and yet these interactions need to be broken to enable scaffolding removal during DNA packaging. To understand the switch at the molecular level, it is necessary to identify the region of the scaffolding protein that interacts with the coat protein subunits and the conformational changes in both of these sites during assembly and exit. In the case of bacteriophage P22, molecular dissection revealed that the recognition domain was located at the C terminus of the scaffolding protein and the NMR structure of this region revealed that it adopted an H-L-H structure in solution (Parker et al. 1998; Sun et al. 2000). The crystal structure of the N-terminal 33 residues of Ø29 scaffolding protein revealed a similar structure, leading to the suggestion that this was the coat protein binding site (Morais et al. 2003).

To identify the region of the Ø29 scaffolding that interacts with the capsid protein, we performed comparative hydrogen/deuterium exchange experiments on free and procapsid-bound scaffolding protein. The observed differences in exchange behavior were localized to the N-terminal H-L-H region, supporting the suggestion of Morais and colleagues that this region is involved in capsid binding. The structural homology between this H-L-H motif and that found in the C-terminal capsid binding domain of the bacteriophage P22 scaffolding protein suggests that they may represent conserved binding motifs as recent studies suggest a common origin of viruses across a striking evolutionary distance (Bazinet and King 1985).

In an effort to identify the residues involved in scaffolding/capsid protein interactions, Lee and Guo (1995) constructed E92Q, D93N, and E95Q mutations in scaffolding protein in an *E. coli* system expressing the scaffolding, capsid, head fiber, and connector genes. With wild-type scaffolding protein, this system results in the formation of procapsid-like particles. However, scaffolding protein carrying mutations in residues 92, 93, and 95 had a deleterious effect on procapsid assembly. While the investigators interpreted these results as implying that residues 92, 93, and 95 interact directly with the capsid protein, the exchange profile of residue 89–94 had no detectable differences in free and procapsid-bound form. Thus it is possible that these mutations

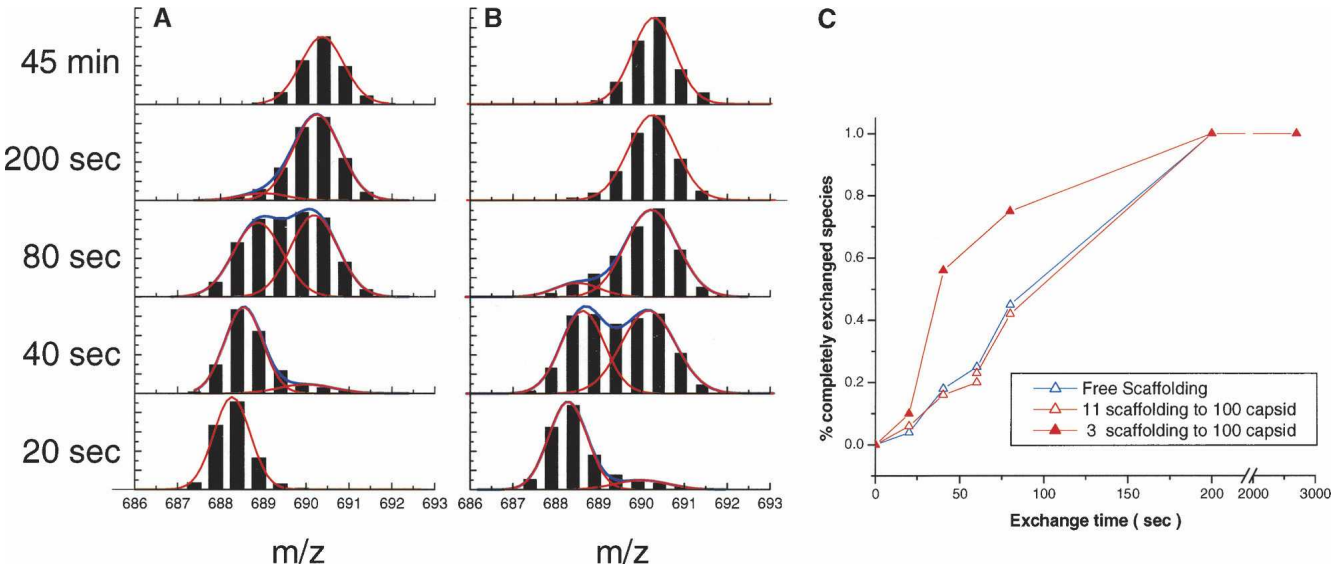

Figure 8. The opening kinetics of free and procapsid-bound scaffolding protein. The isotopic distributions of residues 20–31 in recombinant scaffolding proteins (*A*) and procapsid particles with a 3:100 scaffolding:capsid protein ratio (*B*). The Gaussian approximations are shown in red and blue for individual and the sum of two envelopes. (*C*) The percentage of area under higher mass envelope vs. exchange time for free recombinant scaffolding (blue) and scaffoldings inside procapsids with either a 3:100 (closed red) or 11:100 (open red) scaffolding:capsid ratio.

act indirectly, perhaps by influencing protein folding or self-association. A surprising finding was that the N-terminal H-L-H region displayed a cooperative opening motion. The correlated motions were clearly revealed in the exchange mass spectra of the whole protein as bimodal exchange patterns, and the regions involved in the cooperative motions were subsequently localized by observing bimodal exchange in the peptic fragments. For correlated, or EX1-type exchange, the rate of exchange corresponds to the opening rate of the cooperative unit. The agreement between the opening rates of the individual peptides within the H-L-H motif suggests that the entire H-L-H motif opens in a cooperative movement. Consistent with this suggestion is the fact that approximately one-third of the amide proteins in each of the helical segments exchange in the bimodal component. Presumably, this subset represents the amide protons on the face of the helix that points toward the inside of the H-L-H motif where the local motions are damped by interface packing in the closed state. Under these conditions, exchange via cooperative opening dominates. However, at lower temperature or when H-L-H is tethered, the cooperative exchange is blocked and the exchange through low energy fluctuations (EX2) once again becomes apparent. The introduction of point mutations designed to destabilize hydrophobic interactions into the residues pointing toward the inside of the H-L-H was sufficient to alter the kinetics of the cooperative opening motion, suggesting that it is the hydrophobic packing of these side chains that stabilizes the H-L-H in the closed position.

The structural information of the scaffolding protein inside the procapsid at high resolution is limited to cryo-electron microscopy-based reconstructions (Fane and Prevelige 2003). For Ø29 these reconstructions lack sufficient resolution to show the structure of the H-L-H domain but do indicate multi-concentric layers of scaffolding density with only the outermost layer in contact with the procapsid lattice (Tao et al. 1998; Morais et al. 2005). At low scaffolding occupancy, the cooperative exchange of residue 20–31 in the H-L-H was enhanced in the procapsid-bound form, suggesting a capsid lattice induced destabilization of this domain. At higher scaffolding occupancy the bimodal exchange became undetectable. This suggests that within procapsid there are procapsid-bound and unbound populations of scaffolding with only the bound fraction undergoing destabilization. Studies done in phage P22 demonstrated the presence of tightly and weakly bound classes of scaffolding in procapsids with only the tightly bound subunits being required for proper assembly in vitro (Prevelige et al. 1993; Parker et al. 2001). One function proposed for scaffolding protein is to displace cellular components from inclusion when building procapsids, thereby reserving the entire procapsid volume for packaged DNA. Data with truncated scaffolding protein suggest that it is also incorporated in a "headful" manner (Earnshaw and Casjens 1980; Parker et al. 1998). Thus, the tightly bound subunits may be required for form determination while the less tightly bound molecules serve to exclude cellular components.

The mechanism of the switch controlling scaffolding protein binding and release has been difficult to resolve because of the challenges associated with determining the structure of both the free and bound form of the scaffolding protein. In many of the dsDNA phage, (e.g., HK97, T4, and P22) there is a pronounced change in the structure of the capsid upon DNA packaging (Prasad et al. 1993; Conway et al. 1995, 2001; Jardine and Coombs 1998; Jardine et al. 1998; Zhang et al. 2000; Jiang et al. 2003). This morphological change arises from conformational changes within the coat protein. In the case of P22, it has been proposed that DNA entry electrostatically drives a domain rearrangement within the coat protein subunit, leading to expansion and loss of the scaffolding binding site (Parker and Prevelige 1998). In Ø29 however, no such conformational change accompanying DNA packaging is evident, leaving the mechanism of scaffolding release obscure (Tao et al. 1998; Wikoff and Johnson 1999). However, Morais et al. (2003) postulated that the interaction of scaffolding protein with DNA during packaging would result in an opening of H-L-H motif. The results in this article demonstrate that this opening motion indeed occurs in both free and bound forms. An alteration in the dynamics of the H-L-H region of Ø29 scaffolding protein upon capsid protein binding suggests this is a site of interaction. The dynamic nature of the H-L-H and its change upon binding suggest that the highly flexible and dynamic properties of this motif might account for the conformational switch and transient interactions, which allows the scaffolding protein to release and recycle as intact molecules.

Materials and methods

Protein preparation

Recombinant scaffolding proteins were expressed in *E. coli* BL21 (DE3) pLysS cells harboring plasmid pARgp7 (Lee and Guo 1995). The proteins were purified with HiTrap Q HP column using a NaCl gradient in 50 mM Tris-HCl (pH 8.0), 1 mM EDTA. The scaffolding proteins eluted at 210 mM NaCl and were subsequently dialyzed against TMS buffer (50 mM Tris-HCl at pH 7.8, 10 mM $MgCl_2$, and 100 mM NaCl). Recombinant scaffolding proteins with the single P2G mutation and the double L3C/N35C mutations were constructed from the pARgp7 plasmid with QuikChange Site-Directed Mutagenesis kit using primers P2G (5′-CTTTAAGAAGG AGATATACATATGGGATTAAAACCAGAAGAACACGA AG-3′), L3C (5′-CTTTAAGAAGGAGATATACATATGCC ATGTAAACCAGAAGAACACGAAG-3′), and N35C (5′-GC TCTTCAACAGCTCAGAGTGTGCTACGGTTCTTTTGTG TCC-3′). The plasmids were transformed to *E. coli* BL21 (DE3) pLysS cells and the proteins were purified as described. The C-terminal truncated mutants Δ 62–97 and Δ 48–97 were constructed by introducing a stop codon to replace residues 62 and 48, respectively, by QuikChange Site-Directed Mutagenesis kit with primers Δ 62–97 (5′-GCCGCTGAAAAAGATGATCT GATCGTGTAAAATAGTAAGC-3′) and Δ 48–97 (5′-CCG AGTACAATGATTTAACAAAATGACATGAAAAGTTAG CCGCTG-3′). The proteins were expressed and purified as described. The mass of all purified proteins was within 2 Da of the expected value as determined by TOF mass spectrometry.

Procapsid particles were produced from infecting nonsuppressor *Bacillus subtilis* strain RD2 with the Ø29 mutant phage sus 8.5(900), sus 16(300), sus 14(1241), and purified on a 10%–40% (w/v) sucrose gradient in TMS buffer at 4°C using a Beckman SW55 at the rotor speed of 45,000 rpm for 55 min. The fractions containing procapsids were pelleted and resuspended in TMS buffer as described (Tao et al. 1998).

H/D exchange mass spectrometry

Recombinant scaffolding protein and procapsid particles were exchanged by 10-fold dilution into TMS buffer in D_2O at final concentrations of 20 μM and 0.1 μM, respectively. The exchange reaction was quenched at various points in time by adding a fourfold volume of 2% formic acid to a final pH of 2.5, and samples were immediately flash-frozen in liquid nitrogen and stored at –80°C until analysis using ESI-TOF mass spectrometry (Micromass LCT). The global exchange data were collected from protein eluted from a C4 trap (Michrom BioResources, Inc.) immersed in an ice bath using an acetonitrile gradient containing 0.1% formic acid. The region specific exchange profiles were obtained by digesting quenched samples with 100 μL of pepsin beads (Pierce) on ice and separated with Spin-X centrifuge filter unit (Costar) before analysis. Peptides were assigned by MS/MS sequencing with Micromass Q-TOF II mass spectrometry.

The protein spectra were approximated with Gaussian distributions using the Origin 6.0 program. The isotopic distributions of peptides were smoothed and centered using MassLynx program and subsequently fitted with Gaussian distribution.

To derive the exchange kinetics under EX2 regime, the centroid of the isotopic distribution was calculated at each time point and the progress curve was fitted as a sum of exponentials using up to three terms to classify residues to fast ($k > 1$ min^{-1}), medium ($1\ min^{-1} > k > 0.01\ min^{-1}$), and slow ($k < 0.01$ min^{-1}) exchanging categories.

$$D = N - a\exp(-k_1 t) + b\exp(-k_2 t) + c\exp(-k_3 t)$$

N is the number of exchangeable protons. The values of a, b, and c represent the number of proton that is classified to the category with exchange rate k_1, k_2, and k_3, respectively. The value of D is the total deuteron uptake in the exchange time t.

Analytical ultracentrifugation

Sedimentation equilibrium experiments on wild type, Δ 62–97, and Δ 48–97 scaffolding were done at 25 μM, 10 μM, and 5 μM in TMS buffer at 20°C. The data were collected with Beckman Optima XL-A analytical ultracentrifuge at OD 230 nm at rotor speeds of 28,000 rpm, 33,000 rpm, 37,000 rpm, 46,000 rpm, and 50,000 rpm, respectively. The partial specific volume was calculated by amino acid sequence and the solvent density was calculated by solvent composition using the Sednterp program. The SedAnal 4.02 program (Stafford and

Sherwood 2004) was used to fit the data globally to obtain the molecular weight and dissociation constant.

Electronic supplemental material

Sedimentation equilibrium data of wild type, Δ 62-97 and Δ 48-97 scaffolding proteins.

Acknowledgments

This work was supported by the NIH (GM47980). We thank Dr. Paul Jardine for Ø29 clones and helpful discussions.

References

Bazinet, C. and King, J. 1985. The DNA translocating vertex of dsDNA bacteriophage. *Annu. Rev. Microbiol.* **39:** 109–129.

Berger, B., Shor, P.W., Tucker-Kellogg, L., and King, J. 1994. Local rule-based theory of virus shell assembly. *Proc. Natl. Acad. Sci.* **91:** 7732–7736.

Canet, D., Last, A.M., Tito, P., Sunde, M., Spencer, A., Archer, D.B., Redfield, C., Robinson, C.V., and Dobson, C.M. 2002. Local cooperativity in the unfolding of an amyloidogenic variant of human lysozyme. *Nat. Struct. Biol.* **9:** 308–315.

Casjens, S. and Hendrix, R. 1988. Control mechanisms in dsDNA bacteriophage assembly. In *The bacteriophages* (ed. R. Calendar), pp. 15–19. Plenum Press, New York.

Casjens, S. and King, J. 1975. Virus assembly. *Annu. Rev. Biochem.* **44:** 555–611.

Caspar, D.L. and Klug, A. 1962. Physical principles in the construction of regular viruses. *Cold Spring Harb. Symp. Quant. Biol.* **27:** 1–24.

Chung, E.W., Nettleton, E.J., Morgan, C.J., Gross, M., Miranker, A., Radford, S.E., Dobson, C.M., and Robinson, C.V. 1997. Hydrogen exchange properties of proteins in native and denatured states monitored by mass spectrometry and NMR. *Protein Sci.* **6:** 1316–1324.

Conway, J.F., Duda, R.L., Cheng, N., Hendrix, R.W., and Steven, A.C. 1995. Proteolytic and conformational control of virus capsid maturation: The bacteriophage HK97 system. *J. Mol. Biol.* **253:** 86–99.

Conway, J.F., Wikoff, W.R., Cheng, N., Duda, R.L., Hendrix, R.W., Johnson, J.E., and Steven, A.C. 2001. Virus maturation involving large subunit rotations and local refolding. *Science* **292:** 744–748.

Cordier, F. and Grzesiek, S. 2002. Temperature-dependence of protein hydrogen bond properties as studied by high-resolution NMR. *J. Mol. Biol.* **317:** 739–752.

DiIanni, C.L., Stevens, J.T., Bolgar, M., O'Boyle II, D.R., Weinheimer, S.P., and Colonno, R.J. 1994. Identification of the serine residue at the active site of the herpes simplex virus type 1 protease. *J. Biol. Chem.* **269:** 12672–12676.

Dokland, T. 1999. Scaffolding proteins and their role in viral assembly. *Cell. Mol. Life Sci.* **56:** 580–603.

Earnshaw, W.C. and Casjens, S.R. 1980. DNA packaging by the double-stranded DNA bacteriophages. *Cell* **21:** 319–331.

Fane, B.A. and Prevelige Jr., P.E. 2003. Mechanism of scaffolding-assisted viral assembly. *Adv. Protein Chem.* **64:** 259–299.

Ferraro, D.M., Lazo, N.D., and Robertson, A.D. 2004. EX1 hydrogen exchange and protein folding. *Biochemistry* **43:** 587–594.

Hernandez, H. and Robinson, C.V. 2001. Dynamic protein complexes: Insights from mass spectrometry. *J. Biol. Chem.* **276:** 46685–46688.

Hilton, B.D. and Woodward, C.K. 1979. On the mechanism of isotope exchange kinetics of single protons in bovine pancreatic trypsin inhibitor. *Biochemistry* **18:** 5834–5841.

Homa, F.L. and Brown, J.C. 1997. Capsid assembly and DNA packaging in herpes simplex virus. *Rev. Med. Virol.* **7:** 107–122.

Hoofnagle, A.N., Resing, K.A., and Ahn, N.G. 2003. Protein analysis by hydrogen exchange mass spectrometry. *Annu. Rev. Biophys. Biomol. Struct.* **32:** 1–25.

Jardine, P.J. and Coombs, D.H. 1998. Capsid expansion follows the initiation of DNA packaging in bacteriophage T4. *J. Mol. Biol.* **284:** 661–672.

Jardine, P.J., McCormick, M.C., Lutze-Wallace, C., and Coombs, D.H. 1998. The bacteriophage T4 DNA packaging apparatus targets the unexpanded prohead. *J. Mol. Biol.* **284:** 647–659.

Jiang, W., Li, Z., Zhang, Z., Baker, M.L., Prevelige Jr., P.E., and Chiu, W. 2003. Coat protein fold and maturation transition of bacteriophage P22 seen at subnanometer resolutions. *Nat. Struct. Biol.* **10:** 131–135.

Kaltashov, I.A. and Eyles, S.J. 2002. Studies of biomolecular conformations and conformational dynamics by mass spectrometry. *Mass Spectrom. Rev.* **21:** 37–71.

King, J., Lenk, E.V., and Botstein, D. 1973. Mechanism of head assembly and DNA encapsulation in *Salmonella* phage P22. II. Morphogenetic pathway. *J. Mol. Biol.* **80:** 697–731.

Lanman, J. and Prevelige Jr., P.E. 2004. High-sensitivity mass spectrometry for imaging subunit interactions: Hydrogen/deuterium exchange. *Curr. Opin. Struct. Biol.* **14:** 181–188.

Lee, C.S. and Guo, P. 1995. Sequential interactions of structural proteins in phage ϕ 29 procapsid assembly. *J. Virol.* **69:** 5024–5032.

Mandell, J.G., Falick, A.M., and Komives, E.A. 1998. Identification of protein-protein interfaces by decreased amide proton solvent accessibility. *Proc. Natl. Acad. Sci.* **95:** 14705–14710.

Molday, R.S., Englander, S.W., and Kallen, R.G. 1972. Primary structure effects on peptide group hydrogen exchange. *Biochemistry* **11:** 150–158.

Morais, M.C., Kanamaru, S., Badasso, M.O., Koti, J.S., Owen, B.A., McMurray, C.T., Anderson, D.L., and Rossmann, M.G. 2003. Bacteriophage ϕ29 scaffolding protein gp7 before and after prohead assembly. *Nat. Struct. Biol.* **10:** 572–576.

Morais, M.C., Choi, K.H., Koti, J.S., Chipman, P.R., Anderson, D.L., and Rossmann, M.G. 2005. Conservation of the capsid structure in tailed dsDNA bacteriophages: The pseudoatomic structure of ϕ29. *Mol. Cell* **18:** 149–159.

Parker, M.H. and Prevelige Jr., P.E. 1998. Electrostatic interactions drive scaffolding/coat protein binding and procapsid maturation in bacteriophage P22. *Virology* **250:** 337–349.

Parker, M.H., Casjens, S., and Prevelige Jr., P.E. 1998. Functional domains of bacteriophage P22 scaffolding protein. *J. Mol. Biol.* **281:** 69–79.

Parker, M.H., Brouillette, C.G., and Prevelige Jr., P.E. 2001. Kinetic and calorimetric evidence for two distinct scaffolding protein binding populations within the bacteriophage P22 procapsid. *Biochemistry* **40:** 8962–8970.

Prasad, B.V., Prevelige, P.E., Marietta, E., Chen, R.O., Thomas, D., King, J., and Chiu, W. 1993. Three-dimensional transformation of capsids associated with genome packaging in a bacterial virus. *J. Mol. Biol.* **231:** 65–74.

Prevelige Jr., P.E., Thomas, D., and King, J. 1993. Nucleation and growth phases in the polymerization of coat and scaffolding subunits into icosahedral procapsid shells. *Biophys. J.* **64:** 824–835.

Stafford, W.F. and Sherwood, P.J. 2004. Analysis of heterologous interacting systems by sedimentation velocity: Curve fitting algorithms for estimation of sedimentation coefficients, equilibrium and kinetic constants. *Biophys. Chem.* **108:** 231–243.

Sun, Y., Parker, M.H., Weigele, P., Casjens, S., Prevelige Jr., P.E., and Krishna, N.R. 2000. Structure of the coat protein-binding domain of the scaffolding protein from a double-stranded DNA virus. *J. Mol. Biol.* **297:** 1195–1202.

Tao, Y., Olson, N.H., Xu, W., Anderson, D.L., Rossmann, M.G., and Baker, T.S. 1998. Assembly of a tailed bacterial virus and its genome release studied in three dimensions. *Cell* **95:** 431–437.

Wikoff, W.R. and Johnson, J.E. 1999. Virus assembly: Imaging a molecular machine. *Curr. Biol.* **9:** R296–R300.

Zhang, Z., Greene, B., Thuman-Commike, P.A., Jakana, J., Prevelige Jr., P.E., King, J., and Chiu, W. 2000. Visualization of the maturation transition in bacteriophage P22 by electron cryomicroscopy. *J. Mol. Biol.* **297:** 615–626.